sustainability

MDPI

Article

Empirical Design, Construction, and Experimental Test of a Small-Scale Bubbling Fluidized Bed Reactor

Carlos Vargas-Salgado [1,*], Elías Hurtado-Pérez [1], David Alfonso-Solar [2] and Anders Malmquist [3]

[1] Departamento de Ingeniería Eléctrica (DIE), Universitat Politècnica de València, 46022 Valencia, Spain; ejhurtado@die.upv.es
[2] Instituto Universitario de Investigación en Ingeniería Energética (IUIIE), Universitat Politècnica de València, 46022 Valencia, Spain; daalso@iie.upv.es
[3] Department of Energy Technology Heat and Power Division, Royal Institute of Technology—KTH, 10044 Stockholm, Sweden; andmal@kth.se
* Correspondence: carvarsa@upvnet.upv.es; Tel.: +34-963-877-000

Abstract: The methods currently used for designing a fluidized bed reactor in gasification plants do not meet an integrated methodology that optimizes all the different parameters for its sizing and operational regime. In the case of small-scale (several tens of kWs biomass gasifiers), this design is especially complex, and, for this reason, they have usually been built in a very heuristic trial and error way. In this paper, an integrated methodology tailoring all the different parameters for the design and sizing of a small-scale fluidized bed gasification plants is presented. Using this methodology, a 40 kWth biomass gasification reactor was designed, including the air distribution system. Based on this design, with several simplified assumptions, a reactor was built and commissioned. Results from the experimental tests using this gasifier are also presented in this paper. As a result, it can be said the prototype works properly, and it produces syngas able to produce thermal energy or even electricity.

Keywords: biomass; gasification; syngas; bubbling fluidized bed; renewable energy

Citation: Vargas-Salgado, C.; Hurtado-Pérez, E.; Alfonso-Solar, D.; Malmquist, A. Empirical Design, Construction, and Experimental Test of a Small-Scale Bubbling Fluidized Bed Reactor. *Sustainability* **2021**, *13*, 1061. https://doi.org/10.3390/su13031061

Received: 11 November 2020
Accepted: 15 January 2021
Published: 20 January 2021

1. Introduction

Biomass gasification is one of the most promising technologies for converting biomass into a fuel; it is a relatively clean process able to produce syngas, which can be used as a fuel. The energy from biomass has solved two fundamental problems that plague other forms of renewable energy, such as solar and wind power: the difficulty of storage energy and the capacity of producing energy when it is needed. Biomass can be easily stored, guaranteeing the continuity of energy supply and availability. The low Sulfur content and the high volatile matter of most types of lignocellulosic biomass increase the advantages of its gasification process [1].

Biomass gasification involves a series of endothermic reactions supported by the heat produced from combustion reactions or other heating methods. Through a series of chemical reactions, it yields combustible synthesis gases, such as H_2, CO, and CH_4 [2]. The gasification process has been used for different application areas, such as power generation, gaseous and liquid fuel production, or the chemical sector. The generation of quality syngas with a high heating value depends on the high H_2 and CO content as well as the high fuel conversion ratio and gas efficiency.

The adequate design of fluidized bed reactors is important for the thermochemical decomposition of biomass due to the high rate of heat and mass transfer, along with the ability to separate the solid products from the volatile components produced during the operation. Biomass particles, due to their peculiar shapes, sizes, and densities, cannot be uniformly mixed without a fluidizing medium, such as sand, in a fluidized bed reactor.

The sand acts as a heat vector, distributing the necessary heat; the continued movement of this material ensures the maintenance of isothermal conditions of the bed, preventing the formation of hot spots and increasing the efficiency of the process [3].

Nowadays, the gasifier method design used involves both process and components selection, in addition to optimization. Through the process, it is possible to obtain the quality and quantity of syngas, operation conditions, and preliminary size of the reactor. The selection of components involves structural and mechanical components, mainly the intake system and reactor body. The usual process design includes design specification, mass balance, and momentum and energy balance. The production gas prediction uses stoichiometric and non-stoichiometric models. In the case of the Bubbling fluidized Bed (BFB) reactor, the cross-sectional area, reactor height, and the freeboard height are required as a result [4]. According to the process design, to project a gasification plant, simulation models, such as thermodynamic equilibrium, kinetic equilibrium, CFD (Computational fluid dynamics), and ANN (Artificial neuronal network), are used. In this context, several scientific works for designing a gasification plant have been published [5–14]. Some models give information about one part of the plant, such as reactor, syngas cleaning system, among others (Feeding system, control system, residue removal system, etc.).

In the case of the reactor design, several studies analyzed how is the behavior of the BFB gasification process is and how the reactor design is affected by bed material [15–17], bed agglomeration [18–22], gasifying agent [9,10,23–26], use of catalysts [20,27,28], hydrodynamics [2,29], biomass segregation [5,30], kind and size of biomass [25,30–35], temperature conditions[32,36], or gasification process [37–39]. Results from the experimental test were also studied in [23,24,33,34,40–42], and finally, other publications integrated models and tests to validate simulations [43,44]. In addition, some reviews compared researcher works carried out in the biomass gasification field [31,45–47].

The models and simulation methods mentioned have scientific rigor. In complex processes, such as gasification, the methodology analyzed so far is an option to have a complete design solution, but in practice, it is very difficult to bring it to reality, taking time and effort to obtain a functional solution. Furthermore, sometimes there is a gap between simulation and the construction and commissioning of the reactor. In any case, the gasification reactor design is always a complex process. This work proposes to give a different solution to carry out an empirical design of a bed biomass gasification (BFB) reactor, simplifying the process design as much as possible, employing information collected from both scientific works and results of experimental tests. The final design has been built, tested, and improved, proving that using the applied methodology, a functional reactor could be obtained as a result.

2. Methodology

The methodology for designing the reactor was based on the step-by-step proceeding shown in Figure 1. Starting from the required power, the syngas Lower Heating Value (LHV), and the efficiency of the process, it is possible to estimate the syngas flow required in the fluidization process and diameters of the reactor. Subsequently, parameters of the fixed and fluidized bed (height, volume, mass, and density) were calculated. The design of this kind of reactor is very complex, and it is not an easy task to find a simplified process. In some steps of the methodology, decisions were made by trial. Hence, some design decisions were empirically deduced. As a result, a simplified methodology was obtained. Applying the methodology, the design was carried out, and the reactor was built and tested, obtaining feedback to improve the design process.

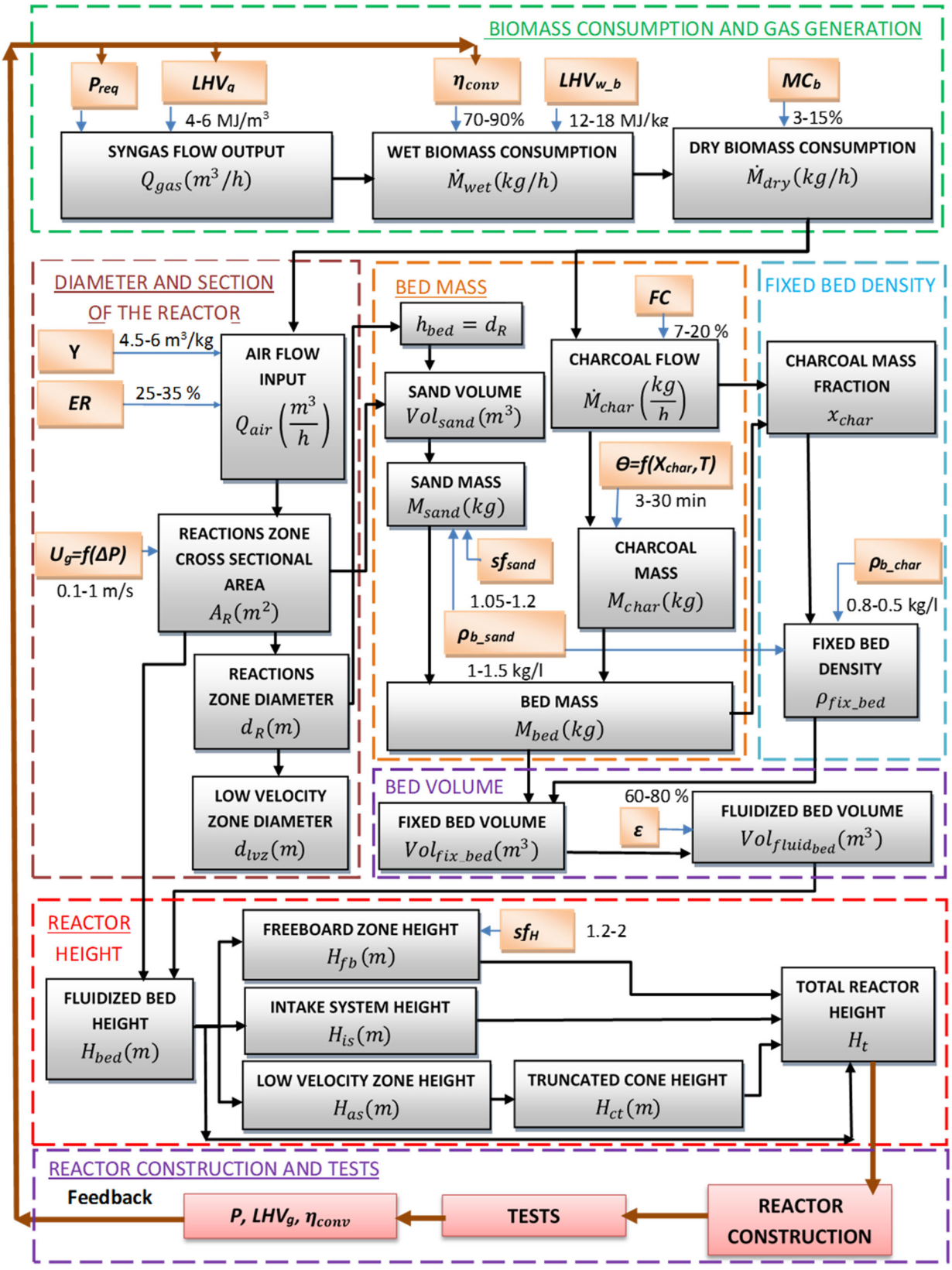

Figure 1. Methodology for designing a bubbling fluidized bed biomass gasification reactor.

2.1. Inputs

The syngas is produced using, as a primary fuel, biomass that is mixed with a gasifying agent (Air). The LHV of the syngas was obtained from the tests carried out in a fluidized bed biomass gasification (BFB) pilot plant. The results obtained correspond to those values shown in the literature [3,48–53]. According to the test, the syngas LHV ranges from 5000 to 6000 kJ/Nm^3. For the design, a value of 5000 kJ/Nm^3 was chosen as an input.

The conversion efficiency from biomass into syngas in the gasification process was determined based on scientific literature [16,26,33,42,54]. For the calculations, a value of efficiency equal to 70% was chosen. The starting parameters for calculations are resumed in Table 1 and they are consistent with the cited bibliography.

The characteristics of biomass (Table 2) have been obtained from experimental tests carried out in the laboratory (LabDER).

Table 1. Starting parameters for the design.

Required Output	40 kWth
Syngas Lowe Heating value	5000 kJ/Nm^3
The efficiency of dry biomass conversion into syngas	70%

Source: [3,16,26,33,42,44,48–54]

Table 2. Characteristics of biomass.

	Type of Biomass	Pellets
	Length (mm)	10–20
	Diameter (mm)	6
Density	Dry biomass (kg/m^3)	1379
	Stored biomass (kg/m^3)	1470
Bulk density	Dry biomass (kg/m^3)	655
	Stored biomass (kg/m^3)	699
	Char (kg/m^3)	304
LHV (kJ/kg)	Dry biomass (kJ/kg)	17,800
	Stored biomass (kJ/kg)	16,700
Ultimate analysis %	C	51.9%
	H	6.2%
	O	41.7%
Proximate analysis %	Fixed carbon (FC)	15.5%
	Volatile	80.5%
	Ash	1.3%
	Moisture (MC)	6.2%

(Source: Test in LabDER).

2.2. Biomass Consumption and Syngas Output

From the required thermal power and the LHV of syngas, it was possible to estimate the quantity of biomass and gasifying medium required. The flow of the produced syngas was determined by entering these values in Equation (1).

$$\dot{Q}_{gas} = \frac{P_{req}\ (\mathrm{kW}) \cdot 3600 \left(\frac{\mathrm{s}}{\mathrm{h}}\right)}{LHV_{gas} \left(\frac{\mathrm{kJ}}{\mathrm{m}^3}\right)} \quad (1)$$

The amount of wet biomass (Moisture 6.2%) needed to generate the syngas required is given by Equation (2).

$$\dot{M}_{wet} = \frac{LHV_{gas}\left(\frac{\mathrm{kJ}}{\mathrm{m}^3}\right) \cdot Q_{gas}\left(\frac{\mathrm{m}^3}{\mathrm{h}}\right)}{LHV_{bio}\left(\frac{\mathrm{kJ}}{\mathrm{kg}}\right) \cdot \eta_{conv}} \quad (2)$$

Once the wet biomass consumption rate was determined and the moisture was experimentally obtained (Table 2), the dry biomass consumption rate (11.5 kg/h) was calculated using Equation (3).

$$\dot{M}_{dry}\left(\frac{\mathrm{kg}}{\mathrm{h}}\right) = (1 - MC) \cdot \dot{M}_{wet}\left(\frac{\mathrm{kg}}{\mathrm{h}}\right) \quad (3)$$

2.3. Diameter and Cross-Section Calculation

The determination of the cross-sectional area of the reactor required the calculation of the airflow and the fluidizing velocity.

2.3.1. Airflow Required for the Fluidization Process

The airflow to be introduced into the reactor at rated conditions could be deduced by obtaining the air/dry biomass ratio for stoichiometric combustion "*Y*" using Equation (4) [55,56]:

$$Y\left(\frac{\mathrm{Nm}^3}{\mathrm{kg}}\right) = \frac{\mathrm{Air}}{\mathrm{Fuel}} = \frac{137.3}{\rho_{air}}\left(\frac{[C]}{12.011} + \frac{1}{4}\frac{[H]}{1.008} - \frac{[O]}{32.00}\right) \quad (4)$$

The elemental composition of the biomass was obtained from Table 2, and ρ_{air} was equal to 1.19 kg/Nm^3. It was deduced that 5.27 Nm^3 air/kg of biomass was required for total stoichiometric combustion. For gasification processes, the de Equivalence Ratio (*ER*) concept was used, which represents the actual air-to-biomass ratio with respect to total stoichiometric combustion. For design purposes, the ER was fixed as 0.29, then $\dot{Q}_{air}$ was calculated by Equation (5), obtaining as a result of 17.6 m^3/h.

$$\dot{Q}_{air} = \dot{M}_{dry} \cdot Y \cdot ER \quad (5)$$

2.3.2. Fluidization

The BFB gasifier is one of the most popular designs for biomass gasification [57], mainly due to its scalability. It consists of a reactor vessel in which the gasifying agent is introduced upward at a velocity of 0.3 to 1.0 m/s [57,58] to agitate the bed material, which sits at the bottom part of the gasifier.

A complete design methodology, including a BFB reactor, requires key indications to guarantee adequate fluidization conditions in the range of operation of the plant, both at nominal and partial load operation.

The range of operating fluidization velocity should be within the minimum fluidization and terminal velocities [8]. In a BFB reactor, this velocity depends, mainly, on the average particle size, properties of the bed materials, and complex interaction processes between gasifying agent and particles [59]. Geldart's classification [60] places materials into four different groups based on particle diameter and density (concretely difference between particle material density and gasifying agent density). Bed materials pertaining to the same group present similar fluidization characteristics [60].

BFB bed materials are generally silica, alumina, or a mixture of them [61] with a particle size in the range of 100–500 μm. These materials have a high specific heat capacity and can operate at high temperatures (higher than 1000°C), which is a requirement as the typical operating temperature of BFB biomass gasifiers is in the range of 800 to 900 °C [58]. Taking into account the described particle size and density of these materials (in the range of 2000 to 4000 kg/m^3), they can be classified as the GELDART group B [60], which fluidizes homogenously, and bubbles appear as soon as the minimum fluidization

velocity is exceeded [60]. Silica sand is usually employed for biomass gasification [61] however, bed agglomeration can occur due to the interaction between the silica-containing bed material and the inorganic part of the fuel (i.e., ash), especially if the latter contains high amounts of alkali metals and/or chlorine that can lower melting point due to the formation of eutectic mixtures [58]. This work focused on a material called Molochite, which can be produced by the calcination of mined kaolin, and, after that, it is refined, making it a cheaper product [62]. The composition and main properties of used Molochite are included in Table 3.

Table 3. Properties of sand (Molochite).

Composition	Value	Unit
Aluminum oxide—Al_2O_3	42	%
Silicon dioxide—SiO_2	55	%
Iron oxide—Fe_2O_3	1.3	%
Properties		
Density	2700	kg/m^3
Bulk density	1210	kg/m^3
Porosity of sand grain	0	%
Color	Grey	
Maximum use temperature	>1700	°C
Thermal expansion coefficient	4.4×10^{-6}	1/°C

Most of the correlations to predict minimum fluidization velocity were based on the Ergun equation (Equation (6)) [63].

$$Ar = 150 \frac{\left(1-\varepsilon_{mf}\right)^2}{{\varepsilon_{mf}}^3} Re_{mf} + 1.75 \frac{Re_{mf}^2}{\varepsilon_{mf}^3} \quad (6)$$

where Ar is the Archimedes number, Re_{mf} is the Reynolds number for minimum fluidization velocity, and ε_{mf} is the void fraction for minimum fluidization velocity. Calculation of Ar and Re_{mf} was performed following Equations (7) and (8):

$$Ar = \frac{\rho_{air} \cdot \left(\rho_{sand} - \rho_{air}\right) \cdot g \cdot d_p^3}{\mu_{air}^2} \quad (7)$$

$$Re_{mf} = \frac{U_{mf} \cdot d_p \cdot \rho_{air}}{\mu_{air}} \quad (8)$$

where ρ_{air} and ρ_p are the density of air and particles in kg/m^3, g is the acceleration of gravity in m/s^2, d_p is the diameter of the particle, μ_g is the dynamic viscosity of gas (air) in kg/m·s, and U_{mf} is the minimum fluidization gas velocity. However, these equations can be simplified into the Wen and Yu equation [63,64] and the Baeyens and Geldart [17] equation, as included in Equations (9) and (10), respectively.

$$U_{mf1} = \frac{\left(\rho_{sand} - \rho_{air}\right) \cdot g \cdot d_p^2}{1650 \cdot \mu_{air}} \quad (9)$$

$$U_{mf2} = \frac{0.0009 \cdot \left(\rho_{sand} - \rho_{air}\right)^{0.934} \cdot g^{0.934} \cdot d_p^{1.8}}{{\rho_{air}}^{0.066} \cdot \mu_{air}^{0.87}} \quad (10)$$

According to these equations, knowing the air properties (density and dynamic viscosity at 25 °C), a particle diameter of $247 \cdot 10^{-6}$ m and a particle density of 2700 kg/m^3 (see Table 3), the minimum fluidization velocity would be equal to 0.054 m/s (U_{mf1}) and 0.052 m/s (U_{mf2}), respectively.

The fluidization velocity for Molochite was evaluated using an experimental methodology according to the bibliography [60,65]. Experimental tests were performed using the pilot plant shown in Figure 2. A fluidization test was performed monitoring air

velocity and pressure drop through the sand bed (molochite), ΔP_{sand}, at ambient temperature (23–25 °C), where U_{mf} was calculated as the intersection [59] of both straight lines (corresponding to fixed bed and fluid bed pressure drop) observed in Figure 3. The main conclusions of the fluidization test for design purposes are included in Table 4.

The minimum fluidization velocity obtained was 0.051 m/s (Table 4), so very similar to predicted values (U_{mf1} and U_{mf2}). This result was expected according to the consulted bibliography [60,65] for GELDART group B particles. To fix design fluidization velocity, it is important to take into account the effect of temperature in the fluidization velocity and, according to [60,63,65], it has been demonstrated experimentally that higher temperature provides lower minimum fluidization velocity.

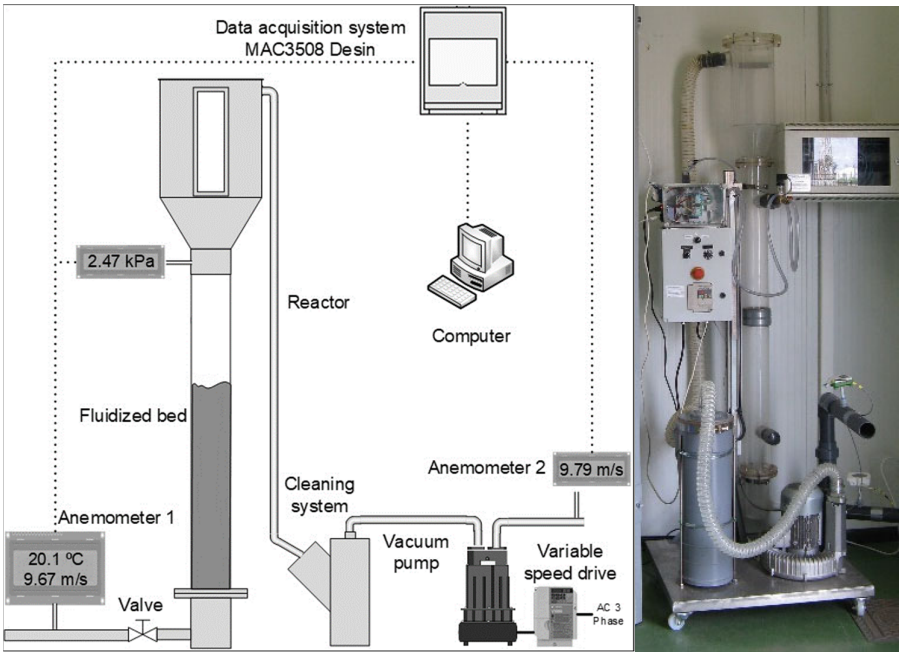

Figure 2. The pilot plant was used to design the air distribution system.

Table 4. Results of the experimental test to calculate the fluidizing velocity.

Average Particle Diameter	d_p	**0.000247 m**
Minimum fluidization velocity for Molochite	U_{mf}	0.051 m/s
Fluidization velocity for design purposes	U_g	0.44 m/s

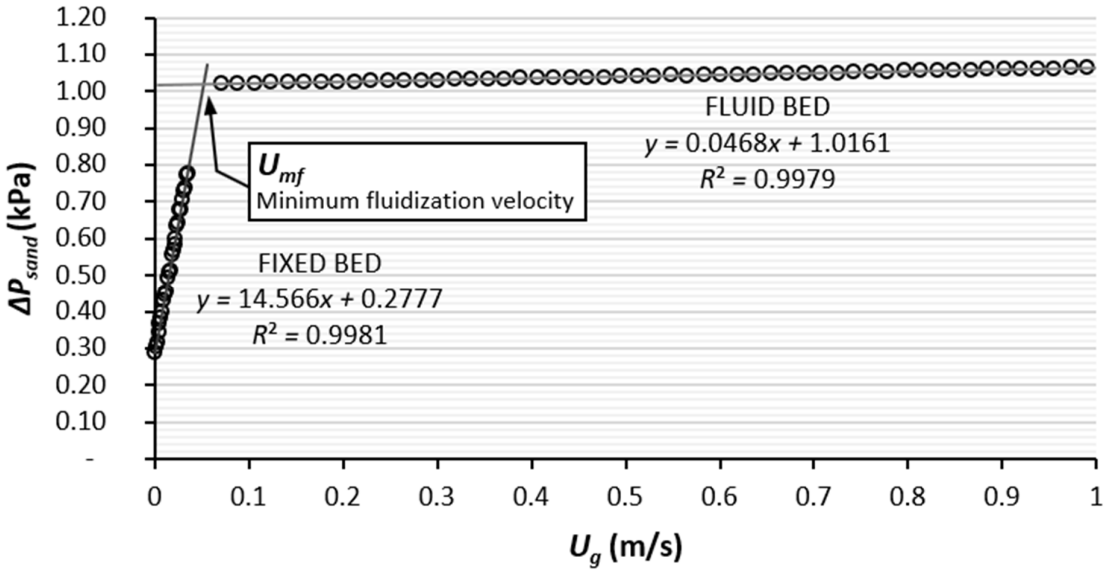

Figure 3. Results of the experimental test carried out to calculate the minimum fluidization velocity for Molochite sand. (Source: tests carried out in LabDER).

To maintain the fluidization of the bed, higher gas velocities were preferred; however, too high velocities could mean that particles are transported out of the reactor. Transport velocity, U_{tr}, is the limit to avoid emptying of the reactor. According to [60] and [65], for silica sand of particle diameter $210 \cdot 10^{-6}$ to $380 \cdot 10^{-6}$ m, U_{tr} (referred to the air inlet velocity) is higher than 2 m/s at ambient temperature (25°C) and higher than 3.5 m/s at temperatures above 600°C. Taking into account that the molochite particle density is even slightly higher than silica sand (2500 kg/m^3), these U_{tr} values can be considered as a valid reference for design purposes and far from design operating fluidization velocities.

The BFB reactor fluidization velocity, U_g, for design purposes, was considered as 0.44 m/s (at rated conditions). It is important to notice that the fluidization velocity at rated conditions was selected to maintain fluidization, also considering partial load operation. At a minimum of 25% of rated capacity, air fluidization velocity would be 0.11 m/s, so still higher than minimum fluidization velocity. Additionally, the U_g value of 0.44 m/s was, at the same time, reasonably far from the transport velocity limit.

It is known that broken bed particles and biomass char or biomass fines can have a lower diameter and lower density than nominal bed material in biomass BFB gasifiers [17]. These particles are usually separated from the gas in cyclones and other gas cleaning systems. However, energy losses due to unreacted biomass in small-scaled BFB gasifiers is lower than 5% according to bibliography [17], which fits with the result shown in Section 3.4, as these losses were 2.5–3%. To partially avoid bed material and unreacted biomass char escaping from the reactor, a low-velocity zone where gas velocity was reduced 9 times was included due to enlargement of internal diameter as described in Section 2.3.3.

2.3.3. Fluidization Diameter and Cross-Section Determination

The design included two sectional areas: the first one was the lower part of the reactor where reactions take place. The second one, in the upper part, had a larger diameter to decrease the velocity and, therefore, avoid the drag of sand and char particles. The cross-sectional area of the reaction zone was calculated from the values of the gas flow and the fluidization velocity:

$$A_r(\mathrm{m}^2) = \frac{\dot{Q}_{air}\left(\frac{\mathrm{m}^3}{\mathrm{h}}\right)}{U_g\left(\frac{\mathrm{m}}{\mathrm{h}}\right)} \quad (11)$$

The inner diameter (d_{bed}) of the reactor can be calculated from A_R. The diameter of the low velocity (d_{lvz}) zone used in the design of the reactor was three times the diameter of the bed zone, as shown in Equation (11). Smaller ratios could be used, but it must be considered that the lower the syngas velocity in this area, the smaller the char and sand drag.

$$d_{lvz}(\mathrm{m}) = 3 \cdot d_{bed}(\mathrm{m}) \quad (12)$$

2.4. Fluidized-Bed Volume Calculation

Fluidized bed volume was evaluated considering the fixed bed volume (sand + char) and the fluidized bed voidage. To calculate the fixed bed volume; the bed mass (sand + char) and the fixed bed density are required.

2.4.1. Bed Mass

The bed mass was calculated by adding the mass of sand and char, which are in the reactor during operation. Once the inner diameter of the reactor is known, it can be used to estimate the volume that was occupied by the sand. The H_{fix}/d_R ratio in a bubbling fluidized reactor ranged from 0.8 to 1.5 [4,7,42,66]. Using a H_{fix}/d_R ratio equal to 1, the volume of sand was calculated according to Equation (12).

$$Vol_{sand} = A_R \cdot h_{bed} = \pi \cdot \left(\frac{d_R}{2}\right)^2 \cdot h_{bed} \quad (13)$$

The bulk density of the chosen sand is detailed in Table 3.

Then, the sand mass was assessed, considering the volume occupied by the sand and the sand bulk density. Nevertheless, because part of sand could be entrained by the gas or the reactor could be operated with more quantity of sand, a safety factor (SF) was applied. We considered, for design purposes, SF = 1.5.

$$M_{sand} = \rho_{b\_sand} \cdot Vol_{sand} \cdot SF \quad (14)$$

For the calculation of the char mass (M_{char}), the char flow ($\dot{M}_{char}$) and the char residence time were first evaluated. ($\dot{M}_{char}$) was estimated using Equation (15).

$$\dot{M}_{char}\left(\frac{\mathrm{kg}}{\mathrm{h}}\right) = \dot{M}_{dry} \cdot FC \quad (15)$$

where 'FC' is the fixed carbon in the biomass, this value is taken from Table 2.

The char residence time (θ) in the reactor was obtained considering the temperature of operation and the percentage of char conversion in the bed. Figure 4 shows the result, which corresponds to an atmospheric air-blown BFB gasifier, processing wood pellets, as obtained by a fluid-dynamic and fuel-conversion model [67,68]. Figure 4 could be used with relative certainty when lignocellulosic biomass composition, size, and density are similar. If a more accurate result is required to characterize a new kind of biomass, either a methodology base on mathematical models must be applied (As explained by [67,68]) or experimental tests must be carried out. According to bibliography [26,33,42,44] the reactor operation temperature is ranged from 650 to 950 °C. For the design, an average value of 832 °C was used, together with the desired char conversion efficiency of close to 80%. The higher the efficiency, the more conservative the design will be, and the reactor will be bigger and more expensive. Figure 4 shows the effect of temperatures on residence time for different char conversion efficiencies (from 60 to 90%). Using the data from Figure 4, the optimum residence time (θ) could be estimated, and the char mass could be deduced.

$$M_{char}(\text{kg}) = \dot{M}_{char}\left(\frac{\text{kg}}{\text{h}}\right) \cdot \theta(\text{min}) \cdot \left(\frac{1\ \text{h}}{60\ \text{min}}\right) \quad (16)$$

The total bed mass was obtained as a sum of the sand and char masses:

$$M_{bed}\ (\text{kg}) = M_{sand} + M_{char} \quad (17)$$

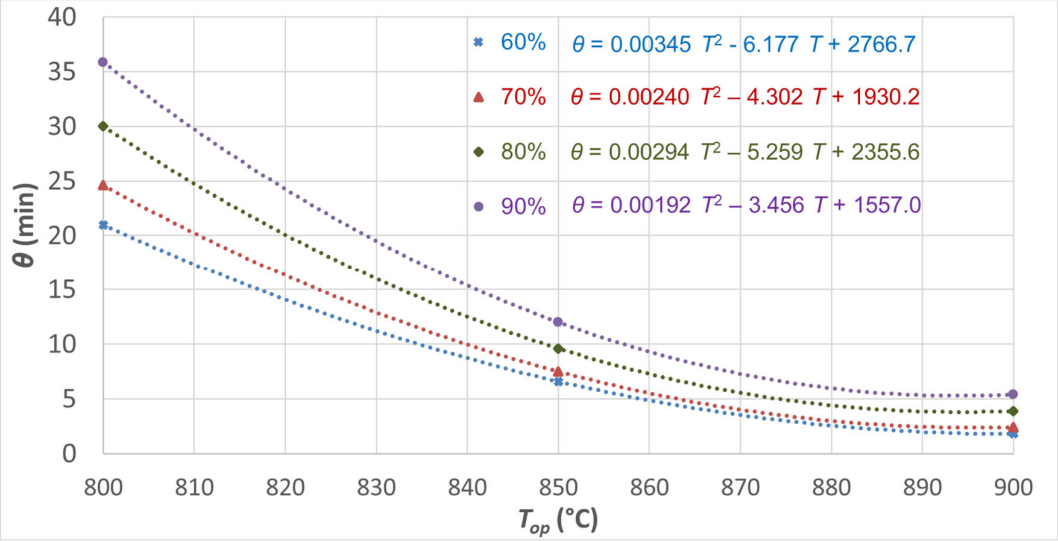

Figure 4. Effect of temperatures on residence time for different char conversion efficiencies [67,68].

2.4.2. Fixed Bed Density

The fixed bed density (ρ_{fix_bed}) is the bulk density of the static bed; it was determined considering the sand bulk density (ρ_{b_sand}), the char bulk density (ρ_{b_char}), and the percentage of reacting char mass with respect to the mass bed (x_{char}). The sand bulk density is shown in Table 3, while the char test results obtained in LabDER are shown in Table 2. The percentage of the reacting char mass in relation to the mass bed (x_{char}) was obtained from the char mass and the sand mass, both calculated previously:

$$x_{char} = \frac{M_{char}(\text{kg})}{M_{fix\_bed}\ (\text{kg})} \quad (18)$$

To obtain the fixed bed density (Static or settled bed), the values calculated previously were replaced in Equation (19).

$$\rho_{b\_fix\_bed} = \rho_{b\_sand} \cdot (1 - x_{char}) + \rho_{b_{char}} \cdot x_{char} \quad (19)$$

2.4.3. Fixed and Fluidized Bed Volume

Once the bed mass (M_{bed}) and the fixed bed density (ρ_{fix_bed}) were deduced, the fixed bed volume was determined by Equation (20).

$$Vol_{fix\_bed}(\text{m}^3) = \frac{M_{bed}\ (\text{kg})}{\rho_{b\_fix\_bed}\left(\frac{\text{kg}}{\text{m}^3}\right)} \quad (20)$$

The voidage fluidized bed value typically ranged from 60 to 80% [2,4,9,49]. Considering the void fraction of the fluidized bed 'ε' equal to 70%, the fluidized bed volume was calculated by Equation (21).

$$Vol_{fluid\_bed}(\text{m}^3) = \frac{Vol_{fix\_bed}(\text{l})}{(1 - \varepsilon)} \quad (21)$$

2.5. Reactor Height Calculation

Following the model used by [4], the bubbling fluidized bed height could be calculated by Equation (22).

$$H_{bed}(\mathrm{m}) = \frac{Vol_{fluid_{bed}}(\mathrm{m}^3)}{A_R(\mathrm{m}^2)} \quad (22)$$

To prevent char and sand bed particles escaping and to ensure the char residence time, a freeboard height was added to the height of the bubbling fluidized bed. Thus, the freeboard height was 0.3 times the bubbling fluidized bed height (H_{bed}), according to Equation (23).

$$H_{fb}(\mathrm{m}) = 0.3 \cdot H_{bed}(\mathrm{m}) \quad (23)$$

Good results were obtained using the height of the low-velocity zone equal to 0.7 times the fluidized bed height (Equation (24)).

$$H_{lvz}(\mathrm{m}) = 0.7 \cdot H_{bed}(\mathrm{m}) \quad (24)$$

A truncated cone joined the area of the fluidized bed and the low-velocity zone, which was a quarter of the height of the low-velocity area (Equation (25)).

$$H_{tc}(\mathrm{m}) = \frac{H_{lvz}(\mathrm{m})}{4} \quad (25)$$

The intake system height was one-third of the fluidized bed height (Equation (26))

$$H_{is}(\mathrm{m}) = \frac{H_{bed}(\mathrm{m})}{3} \quad (26)$$

Adding up all the values previously obtained, the total height of the reactor was (Equation (27)).

$$H_T(m) = H_{bed} + H_{fb} + H_{tc} + H_{lvz} + H_{is} \quad (27)$$

2.6. Distributor Design

To obtain adequate fluidization, besides choosing the right sand, an appropriate distributor pressure drop was also required. To choose the right distributor, several tests were conducted employing different holed plates for the reactor intake system. The prototype used to carry out the test is shown in Figure 2. A picture of a holed plate used for the distributor system is shown in Figure 5.

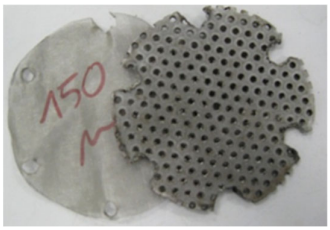

Figure 5. Picture of one of the holed plates and one of the meshes used for the distribution system test.

Tests to modify the pressure drop in the air admissions systems were carried out to estimate the adequate distributor pressure drop (ΔP_{dist}). To modify the total pressure drop (ΔP_{total}), which was equal to ΔP_{dist} plus the sand pressure drop (ΔP_{sand}), a valve was used (Figure 2) to simulate ΔP_{dist}. To carry out the tests, a metallic mesh with neglected pressure drop (an open area close to 36%) was used at the bottom part to keep the sand into the reactor. Once the sand was introduced and the valve was completely open, the vacuum pump was turned on. The valve was gradually closed until reaching a point at which,

keeping constant the airflow at 17.6 m³/h, oscillations were drastically reduced (ΔP_{tot} min in Figure 6). This was considered the minimum ΔP_{total} to work properly. After that, the valve was partially closed a bit more until reaching a second position, corresponding to the maximum ΔP_{total}. (ΔP_{tot} max in Figure 6). Finally, to estimate ΔP_{dist}, the valve was set to the optimal point (ΔP_{tot} opt in Figure 6), where the pressure oscillations were the lowest. Then, removing the sand from the reactor and introducing 17.6 m³/h of air, ΔP was directly measured, obtaining ΔP_{dist} for each point (Figure 6). As a result, the ΔP_{total} range as a function of the sand introduced into the reactor was estimated, as shown in Figure 6. It must be notified that for constant airflow, the right ΔP_{dist} depends on the H_{fix}/d_R ratio. The tests were carried out for different H_{fix}/d_R ratios (0.25, 0.5, 0.75 and 1, 1.15—Figure 6).

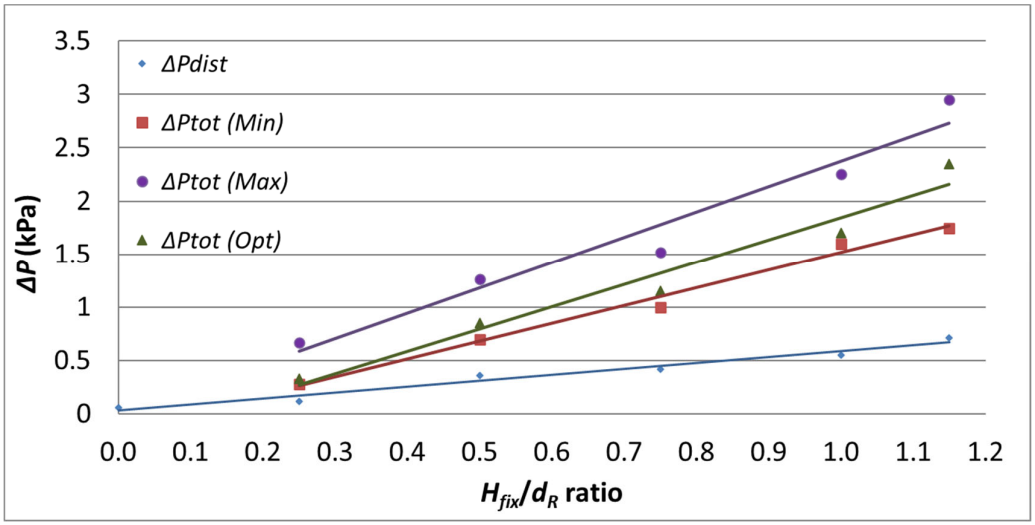

Figure 6. Proper range of ΔP_{tot} and ΔP_{dist} as a function of the H_{fix}/d_R ratio.

To find the right distributor (regardless of the valve), the characterization of the distributor plate as a function of ΔP_{dist} was required. For that purpose, several plates with 1 mm diameter holes and different holed areas (and different pressure drops) were tested, as shown in Figure 7. In this manner, through the desired ΔP_{dist}, it was possible to choose the required holed area of the distributor plate.

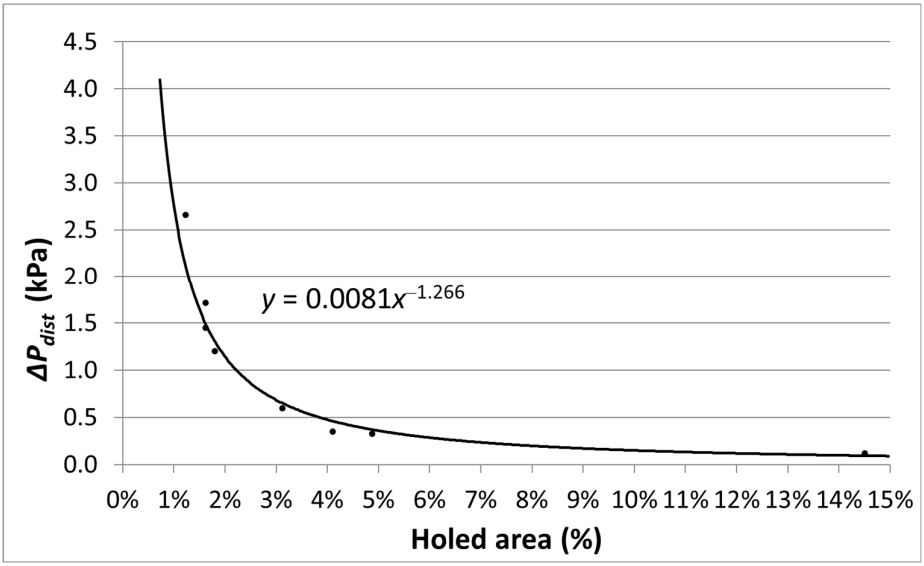

Figure 7. Distribution plate pressure drop as a function of the plate holed area.

3. Results

3.1. Construction

Selected materials for the reactor manufacturing must withstand the oxidizing and reducing atmospheres in which the reactions take place, as well as high operating temperature. Moreover, an optimal solution should also consider materials with a convenient cost–benefit ratio. In this regard, the stainless steel AISI type 310 meets most of the required characteristics. Ceramic coating can be used in the reactions zone of the reactor; however, the reactor would be more fragile to the thermal expansion of the two different materials, and this option would increase the cost and maintenance of the reactor. The results of applying the methodology are shown in Table 5. Figure 8 presents a drawing of the deduced system.

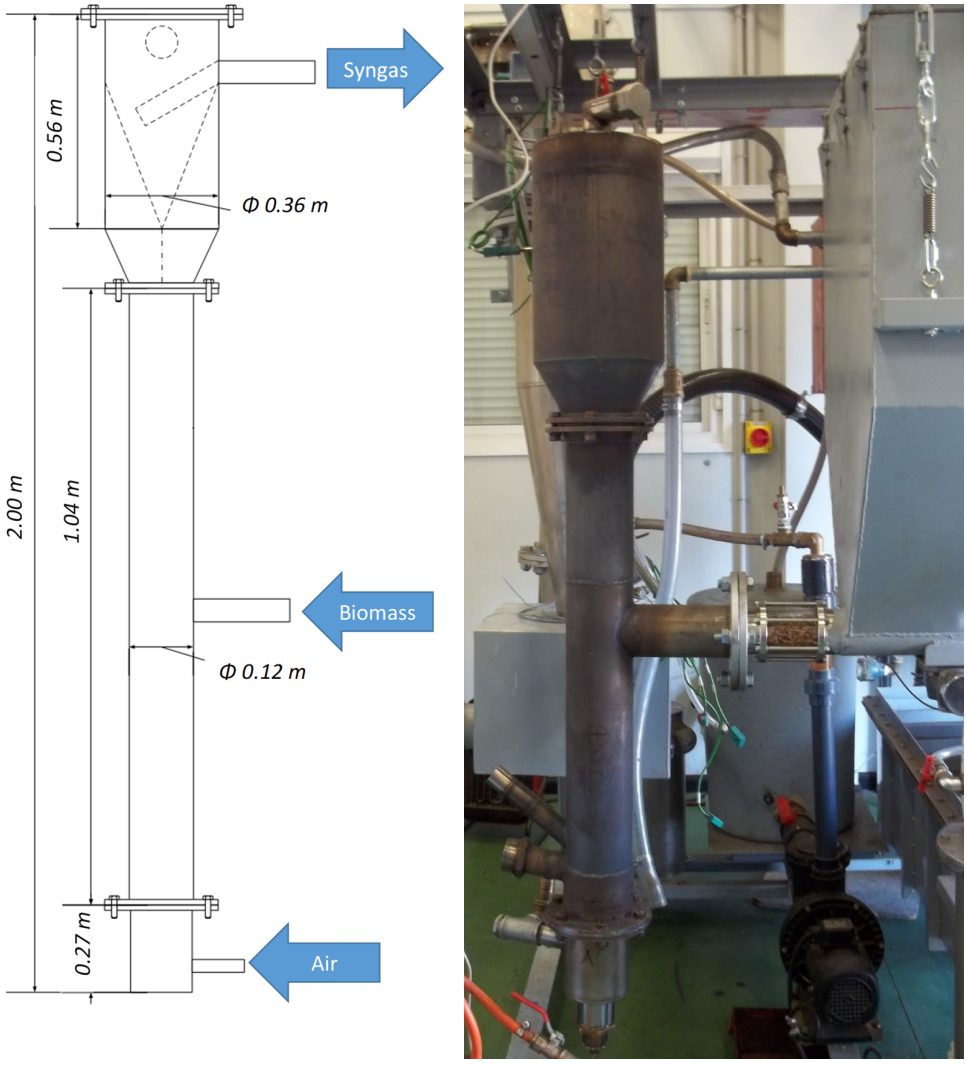

Figure 8. Drawing and picture of the reactor.

Given that working temperature was in the range of 750 to 920°C, an AISI type 310 austenitic stainless steel, which is a medium carbon used for high-temperature applications (up to 1035°C in continuous service, and 1150°C for intermittent operation [69]), AISI type 310 austenitic stainless steel was used for the construction of the reactor. According to the experimental tests conducted in LabDER, when bed temperature was well controlled, satisfactory results could be obtained with such material.

Table 5. Reactor Dimensions.

The inner diameter of the reactions zone	d_R	**0.12 m**
The cross-sectional area of the reactions zone	A_R	0.0113 m^2
The inner diameter of the low-velocity zone (Upper part)	d_{lvz}	0.34 m
Bubbling fluidized bed height	H_{bed}	0.8 m
Reaction zone freeboard height	H_{fb}	0.24 m
Reactions zone height (Sum of two previous)	H_{rz}	1.04 m
Low-velocity zone height	H_{lvz}	0.56 m
Truncated cone height	H_{tc}	0.14 m
Intake system height	H_{is}	0.27 m
Height of the reactor	H_R	2 m

3.2. Air Intake System

According to Figure 6 and working with a H_{fix}/d_R ratio equal to 1, ΔP_{dist} must be equal to 0.55 kPa. Thereby, to reach adequate fluidization, and according to Figure 7, the holed area of the distributor plate (%H) must be close to 3%. To reach the desired configuration, a holed plate with 300 holes 1 mm diameter was used. Figure 9 shows the distribution system.

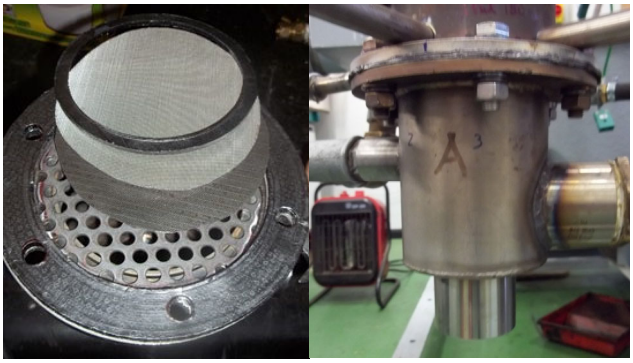

Figure 9. Picture of one of the distribution system configurations used for the tests (**left**) and air admission system (**right**).

3.3. Experimental Tests

Once the reactor was built, preliminary checks for commissioning were completed and, two experimental tests were carried out and analyzed to validate the design. In test 1 (Figures 10 and 11), the load was modified every 5 min. In test 2 (Figures 12 and 13), the load was constantly modified.

Four thermocouples (see Figure 14) to measure temperatures at different heights were installed (T1, T2, T3, and T4 at heights of 0.064 m, 0.228 m, 0.327 m, and 0.428 m from the distributor, respectively). T4 was considered the most representative of the bed since the thermocouple was located in the middle of the fluidized bed. LHV_g was determined by using a portable infrared gas analyzer model Gasboard-3100p Series. Additionally, a syngas flow meter (Rotameter TecFLuid series PT calibrated for syngas) was used to measure the syngas flow. With all these measurements, the energy produced was deduced.

Figures 11 and 12 show the input and output power (calculated from syngas and biomass flow and the heating value of the syngas produced and the biomass used) and the efficiency calculated from the input and the output power. The output power ranged from 15 to 42 kWth, and the instantaneous efficiency ranged from 59 to 82% at continuous operation. It can be noticed, when the load was increased over 41–42 kWth (Figure 12 from

13:24), the temperature decreased, indicating that with this over this load, the power was about to reach the maximum limit for a proper operation of the reactor.

Figure 13 shows the LHV, the air, syngas, and biomass flow obtained in the tests carried out, keeping the load constant at least 5 min. The LHV went from 5000 to 6000 kJ/Nm^3. The biomass flow went from 7 to 10 kg/h. Figure 14 shows the same data when the load was modified every few seconds. The biomass flow ranged from 5 to 13 kg/h, and LHV went from 5000 to 6000 kJ/Nm^3.

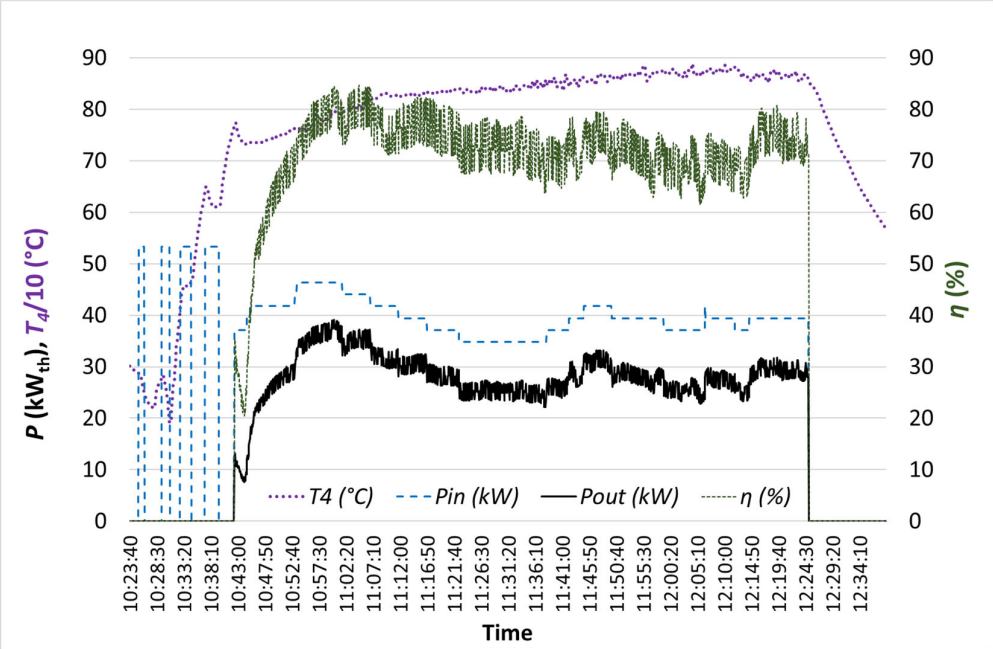

Figure 10. Test 1: Estimation of efficiency keeping constant the load at least 5 min.

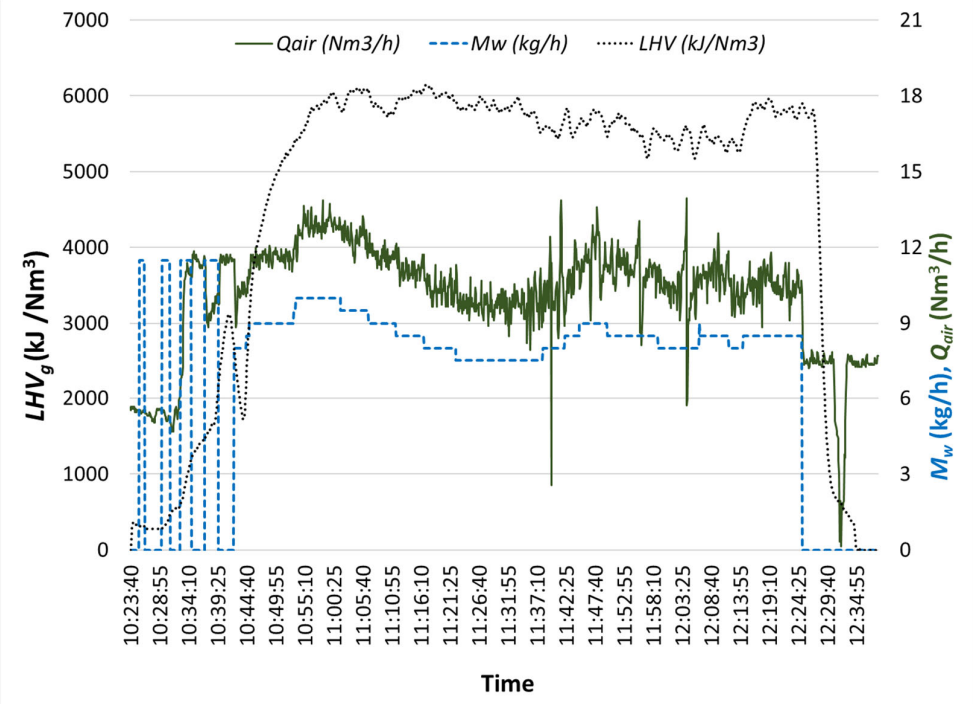

Figure 11. LHV_g, Q_{air}, and Biomass flow obtained from the test 1.

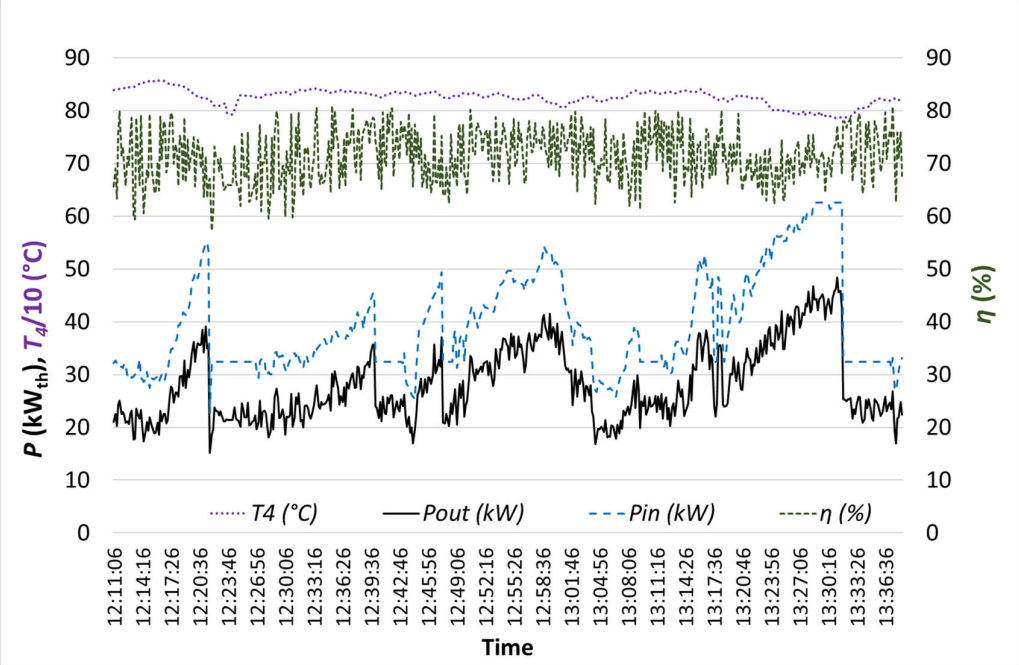

Figure 12. Test 2: Estimation of efficiency modifying constantly the load.

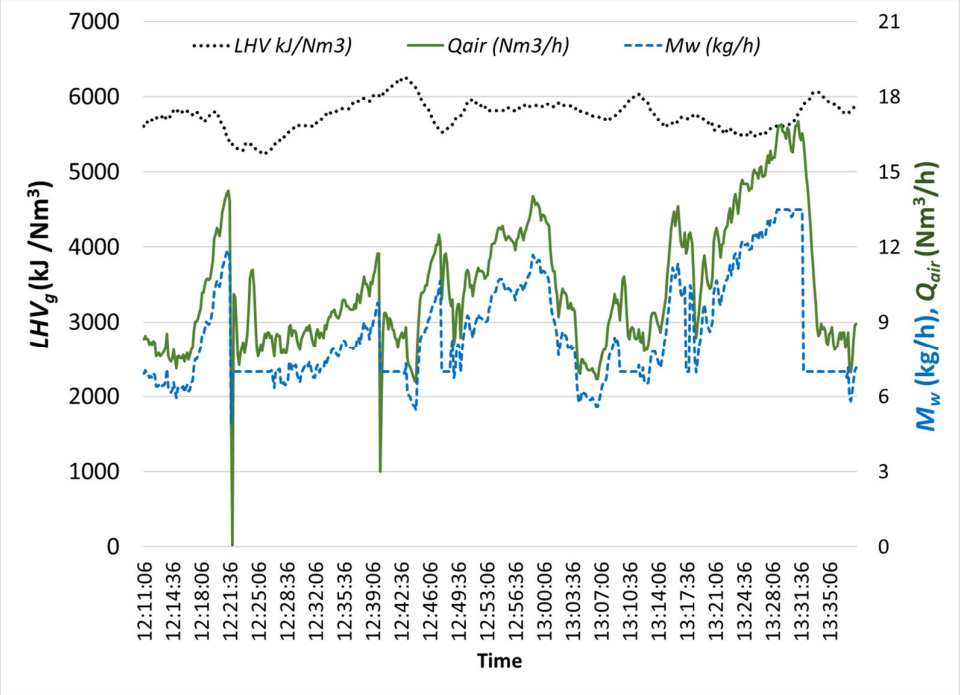

Figure 13. LHV_g, Q_{gas}, Q_{air}, Biomass flow obtained from test 2.

Figure 14. Thermocouples located in a thermowell: Top of the reactor (**Left**), inside the reactor (**Right**).

The maximum temperature was 920°C. High temperatures (Left Figure 15) provoked thermal dilatation of the reactor. The adopted solution for such dilatation was the use of springs, according to Figure 15 (right).

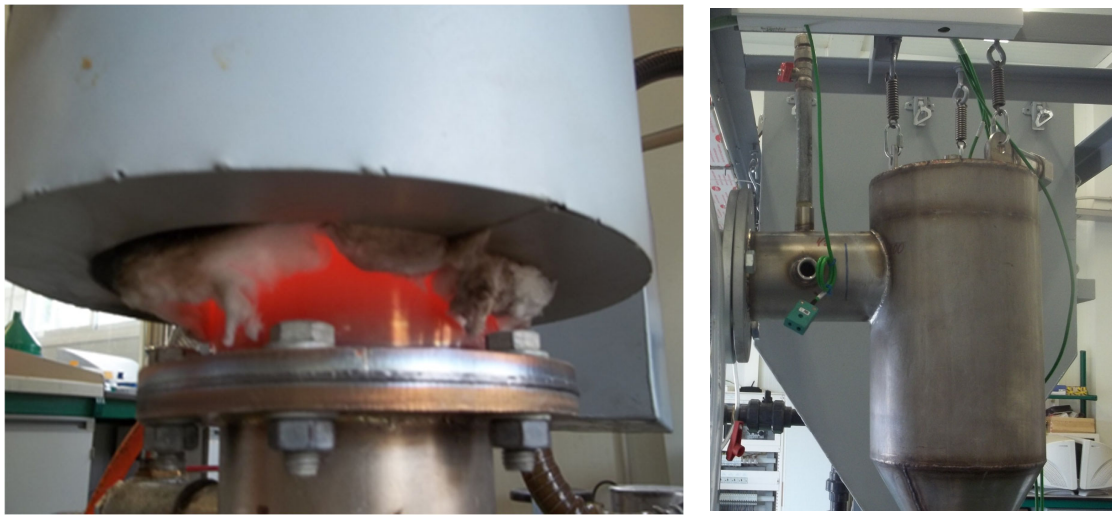

Figure 15. Bottom part of the reactor, when heated to red heat during the operation (**left**), Reactor holder system to absorb thermal expansion (Right).

The datasheet of the reactor is shown in Table 6.

Table 6. Datasheet of the reactor at rated conditions.

Power Output Range	P_{range}	15–42 kWth
Gas lower heating value	LHV_g	5–6 MJ/Nm^3
Wet biomass lower heating value	LHV_{w_b}	16.7 MJ/kg
Syngas flow output	Q_{gas}	10–28 Nm^3/h
Wet biomass consumption	$\dot{M}_w$	5–13 kg/h
Biomass moisture	MC_b	6.2%
Airflow needed for the gasification process	Q_{air}	6–17.6 Nm^3/h

3.4. Performance

The performance of the gasification process is shown in Table 7. The capacity of the reactor to gasify fines from pellets was analyzed from the result of the test. Figure 11 shows the results of a 2 h 25 min test. According to the result of the test, the total consumption of biomass was 17.2 kg (with 6.2% of moisture content). Solids contained in the syngas were separated in a cyclone, and the material collected (Figure 16) weighed 477.3 g. The heating value of the cyclone discharge material (char + ash) was 17.12 MJ/kg; it was estimated through the calorimeter CAL2k ECO. The losses due to unconverted fines were about 8.17 MJ, equivalent to 2.5–3% with respect to the energy input. In addition, moisture and ash content were obtained according to UNE-EN ISO 18134–2:2017 and UNE-EN ISO 18122:2015. Taking into account that the moisture content of the material collected in the cyclone was 0.92% and ash content was 43.56%, it can be deduced that unreacted biomass going out of the reactor was very reduced, and the mass of fines (mainly a mixture of ash and unreacted biomass char), was about 0.028 $kg_{fines}/kg_{biomass}$. This value corresponds to the results shown in [17] for a BFB reactor operating with wood pellets.

Table 7. Performance of the reactor.

		Units	Operating Range—Experimental Test	Range According Scientific Works	Sources
Lower heating value	LHV_g	MJ/Nm^3	5.2–6.2	4.5–6.6	[26,33,44,54]
Equivalence ratio	ER	-	0.26–0.3	0.15–0.35	[33,42,44,66,70]
Syngas yield/biomass		Nm^3/kg	1.9–2.3	1.7–2.5	[33,54]
Bed temperature	T_{op}	°C	792–860	650–950	[26,33,42,44]
Efficiency	η_{conv}	%	59–82	55–88.28	[16,26,33,42,54]

Figure 16. Cyclone discharge material.

4. Conclusions

Customizing the design of a biomass gasification reactor for a specific demand and use is a very complex task. It requires generating an adequate syngas flow to cover power or heat demands. So far, only heuristic approaches based on complex processes and strict criteria have been used for the design of the reactors to be used in a gasification plant. In this paper, a novel simplified design methodology of a BFB biomass reactor, starting from the required thermal power, was presented and design steps were described and justified. Employing this methodology, the complexity of the design, and the time to design and build a small-scale biomass gasification reactor is reduced. Equations for fluidization velocities estimation from the bibliography were presented, applied and compared with experimental data. In this way, the fluidization characteristics of the proposed bed material were validated. A complete procedure to calculate dimensions of the different reactor zones (height and diameter) and suggested construction materials have been included.

The design methodology was applied for a 40 kWth gasification reactor operating with biomass pellets, and a real prototype was constructed and tested. The total height of the reactor was 2 m, and the diameter of the reaction zone was 12 cm.

A review of this type of BFB biomass gasification reactor was made, and operation parameters were aligned with the consulted bibliography. According to experimental tests carried out with this gasification reactor, efficiency ranged from 59 to 82% for an output range power from 15 to 42 kWth.

The assumptions made in the design methodology could introduce a certain level of uncertainty if bed material or biomass type is changed. However, the presented design methodology was experimentally validated with satisfactory results from tests carried out.

5. Nomenclature

A_R	Definitive cross-sectional area (m^2)
A_r	Initial cross-sectional area (m^2)
Ar	Archimedes number
d_R	Definitive inner diameter of the reactor [m)
d_p	Average sand particle diameters, calculated by laboratory test (m)
d_{lvz}	Diameter of the low-velocity zone (m)
ER	Actual biomass/air ratio respect to the stoichiometric biomass/air ratio.
FC	Weight percentage of fixed carbon (%)
H_{bed}	Bubbling bed height (m)
H_{fb}	Reactor freeboard height (m)
H_{fix}	Static or settle height bed (m)
H_{rz}	Reactions zone height (m)
H_{lvz}	Low-velocity zone height (m)
H_{tc}	Truncated cone height (m)
H_{is}	Intake system height (m)
H_t	Total height (m)
ICE	Internal combustion engine
LHV_{w_b}	Wet (without drying) biomass Lower Heating Value (kJ/kg)
LHV_{D_b}	Dry biomass Lower Heating Value (kJ/kg)
LHV_g	Syngas Lower Heating Value (kJ/kg)
M_{bed}	Bed mass (sand + char) (kg)
M_{char}	Char mass into the reactor (kg)
M_{sand}	Sand mass into the reactor (kg)
$\dot{M}_{dry}$	Dry biomass consumption rate (kg/h)
$\dot{M}_{char}$	Mass flow char (kg/h)
$\dot{M}_w$	Wet (without drying) biomass consumption rate (kg/h)
MC_b	Biomass moisture content (%)

P_{req}	Required electrical power (kW)
Q_{air}	Flow of air (Nm^3/h)
Q_{gas}	Flow of syngas (Nm^3/h)
r	ratio air/biomass for the gasification process (Nm^3/kg)
Re_{mf}	Reynolds number at minimum fluidization velocity
sf_a	Area safety factor
sf_{sand}	Sand safety factor
T_{op}	Operating temperature (°C)
U_g	fluidization velocity (m/s)
U_{mf}	minimum velocity (m/s)
U_{mf}	transport velocity (m/s)
Vol_{sand}	Sand volume in fixed bed (m^3)
Vol_{fix_bed}	Fixed bed volume (m^3)
Vol_{fluid_bed}	Fluidized bed volume (m^3)
x_{char}	Reacting char mass respect to mass bed (%)
Y	air/biomass ratio for complete combustion (m^3 air/kg biomass)
ΔP_{total}	Total pressure drop (kPa)
ΔP_{sand}	Sand pressure drop (kPa)
ΔP_{dist}	Distributor pressure drop (kPa)
ρ_{air}	Air density (kg/m^3)
ρ_{syng}	Syngas density (kg/m^3)
ρ_{d_bio}	Dry biomass density (kg/m^3)
ρ_{fix_bed}	Fixed bed density (sand + char) (kg/m^3)
ρ_{fluid_bed}	Fluidized bed density (sand + char) (kg/m^3)
ρ_{b_char}	Char bulk density (kg/m^3)
ρ_{b_sand}	Sand bulk density (kg/m^3)
ρ_{sand}	Sand density (kg/m^3)
ρ_{char}	Char density (kg/m^3)
μ_{air}	dynamic viscosity air (kg/m s)
ε	Voidage of the fluidized bed (%)
ε_{mf}	Voidage of the bed at minimum fluidization velocity (%)
η_{conv}	Cold gas efficiency conversion from biomass into syngas (%)
η_{conv_desir}	Desired efficiency conversion from char into syngas (%)
η_{ice}	Efficiency conversion from syngas to electricity in the internal combustion engine. (%)
Θ	Char residence time (min)
$[C]$	Weight percentage of Carbon (%)
$[H]$	Weight percentage of Hydrogen (%)
$[O_2]$	Weight percentage of Oxygen (%)

Author Contributions: Conceptualization, C.V.-S. and D.A.-S.; methodology, C.V.-S. and E.H.-P.; validation, C.V.-S., E.H.-P. and D.A.-S.; formal analysis, C.V.-S. and D.A.-S.; investigation, C.V.-S. and E.H.-P.; resources, C.V.-S., E.H.-P. and A.M.; data curation, C.V.-S. and D.A.-S.; writing—original draft preparation, C.V.-S., E.H.-P. and D.A.-S.; writing—review and editing C.V.-S. and D.A.-S.; visualization, C.V.-S. and D.A.-S.; supervision, E.H.-P. and A.M.; project administration, E.H.-P.; funding acquisition, E.H.-P. All authors have read and agreed to the published version of the manuscript.

Funding: This work was supported in part by the European Commission through GROW GREEN project (Agreement number: 730283—GROW GREEN—H2020-SCC-2016–2017/H2020-SCC-NBS-2stage-2016. http://growgreenproject.eu/).

Acknowledgments: This work was completed in the framework of the activities of the Renewable Area research group of the IUIIE (Instituto Universitario de Investigación en Ingeniería Energética) in regional, national, and international projects. The authors deeply thank the Universitat Politècnica de València, IMPIVA-Generalitat Valenciana, the Spanish Ministry of Science and Technology, and the European Commission for the funded projects coming from this organization.

Conflicts of Interest: The authors declare no conflict of interest.

References

1. Anukam, A.; Goso, B.P.; Okoh, O.O.; Mamphweli, S.N. Studies on Characterization of Corn Cob for Application in a Gasification Process for Energy Production. *J. Chem.* **2017**, *2017*, 1–9, doi:10.1155/2017/6478389.
2. Yang, S.; Wang, H.; Wei, Y.; Hu, J.; Chew, J. Numerical Investigation of Bubble Dynamics during Biomass Gasification in a Bubbling Fluidized Bed. *ACS Sustain. Chem. Eng.* **2019**, *7*, 12288–12303, doi:10.1021/acssuschemeng.9b01628.
3. Prabir, B. *Biomass Gasification and Pyrolysis. Practical Design and Theory*, 1st ed.; Elsevier Inc.: Amsterdam, The Netherlands, 2010.
4. Basu, P. Combustion and Gasification in Fluidized Beds. In *Combustion and Gasification in Fluidized Beds*; CRC Press: Boca Raton, FL, USA, 2006.
5. Sharma, A.; Wang, S.; Pareek, V.; Yang, H.; Zhang, D. CFD modeling of mixing/segregation behavior of biomass and biochar particles in a bubbling fluidized bed. *Chem. Eng. Sci.* **2014**, *106*, 264–274, doi:10.1016/j.ces.2013.11.019.
6. Nilsson, S.; Gómez-Barea, A.; Fuentes-Cano, D.; Campoy, M. Gasification kinetics of char from olive tree pruning in fluidized bed. *Fuel* **2014**, *125*, 192–199, doi:10.1016/j.fuel.2014.02.006.
7. Fotovat, F.; Abbasi, A.; Spiteri, R.J.; De Lasa, H.; Chaouki, J. A CPFD model for a bubbly biomass–sand fluidized bed. *Powder Technol.* **2015**, *275*, 39–50, doi:10.1016/j.powtec.2015.01.005.
8. Sant'Anna, M.C.S.; Cruz, W.R.D.S.; Da Silva, G.F.; Medronho, R.; Lucena, S. Analyzing the fluidization of a gas-sand-biomass mixture using CFD techniques. *Powder Technol.* **2017**, *316*, 367–372, doi:10.1016/j.powtec.2016.12.023.
9. Yang, S.; Fan, F.; Wei, Y.; Hu, J.; Wang, H.; Wu, S. Three-dimensional MP-PIC simulation of the steam gasification of biomass in a spouted bed gasifier. *Energy Convers. Manag.* **2020**, *210*, 112689, doi:10.1016/j.enconman.2020.112689.
10. Qi, T.; Lei, T.; Yan, B.; Zhou, Z.; Li, Z.; Fatehi, H.; Wang, Z.; Bai, X.-S. Biomass steam gasification in bubbling fluidized bed for higher-H2 syngas: CFD simulation with coarse grain model. *Int. J. Hydrogen Energy* **2019**, *44*, 6448–6460, doi:10.1016/j.ijhydene.2019.01.146.
11. Lim, Y.-I.; Lee, U.-D. Quasi-equilibrium thermodynamic model with empirical equations for air–steam biomass gasification in fluidized-beds. *Fuel Process. Technol.* **2014**, *128*, 199–210, doi:10.1016/j.fuproc.2014.07.017.
12. Xie, J.; Zhong, W.; Jin, B.; Shao, Y.; Liu, H. Simulation on gasification of forestry residues in fluidized beds by Eulerian–Lagrangian approach. *Bioresour. Technol.* **2012**, *121*, 36–46, doi:10.1016/j.biortech.2012.06.080.
13. Agu, C.E.; Pfeifer, C.; Eikeland, M.; Tokheim, L.-A.; Moldestad, B.M.E. Detailed One-Dimensional Model for Steam-Biomass Gasification in a Bubbling Fluidized Bed. *Energy Fuels* **2019**, *33*, 7385–7397, doi:10.1021/acs.energyfuels.9b01340.
14. Kang, P.; Hu, X.E.; Lu, Y.; Wang, K.; Zhang, R.; Han, L.; Yuan, H.; Chen, H.; Luo, X.; Zhou, Y. Modeling and Optimization for Gas Distribution Patterns on Biomass Gasification Performance of a Bubbling Spout Fluidized Bed. *Energy Fuels* **2020**, *34*, 1750–1763, doi:10.1021/acs.energyfuels.9b02512.
15. Serrano, D.; Von Berg, L.; Anca-Couce, A.; Hochenauer, C.; Scharler, R.; Anca-Couce, A. Effect of bed material density on the performance of steam gasification of biomass in bubbling fluidized beds. *Fuel* **2019**, *257*, 116118, doi:10.1016/j.fuel.2019.116118.
16. Bhaird, S.T.M.A.; Hemmingway, P.; Walsh, E.; Maglinao, A.L.; Capareda, S.C.; McDonnell, K. Bubbling fluidised bed gasification of wheat straw–gasifier performance using mullite as bed material. *Chem. Eng. Res. Des.* **2015**, *97*, 36–44, doi:10.1016/j.cherd.2015.03.010.
17. Zaccariello, L.; Mastellone, M.L. Fluidized-Bed Gasification of Plastic Waste, Wood, and Their Blends with Coal. *Energies* **2015**, *8*, 8052–8068, doi:10.3390/en8088052.
18. Bhaird, S.T.M.A.; Walsh, E.; Hemmingway, P.; Maglinao, A.L.; Capareda, S.C.; McDonnell, K. Analysis of bed agglomeration during gasification of wheat straw in a bubbling fluidised bed gasifier using mullite as bed material. *Powder Technol.* **2014**, *254*, 448–459, doi:10.1016/j.powtec.2014.01.049.
19. Kuo, J.-H.; Wey, M.-Y.; Lian, Y.-H.; Samaksaman, U. Gaseous organic emissions during air gasification of woody waste: effect of bed agglomeration/defluidization. *Fuel Process. Technol.* **2014**, *128*, 104–110, doi:10.1016/j.fuproc.2014.07.008.
20. Serrano, D.; Sánchez-Delgado, S.; Sobrino, C.; Marugán-Cruz, C. Defluidization and agglomeration of a fluidized bed reactor during Cynara cardunculus L. gasification using sepiolite as a bed material. *Fuel Process. Technol.* **2015**, *131*, 338–347, doi:10.1016/j.fuproc.2014.11.036.
21. Kittivech, T.; Fukuda, S. Investigating Agglomeration Tendency of Co-Gasification between High Alkali Biomass and Woody Biomass in a Bubbling Fluidized Bed System. *Energies* **2019**, *13*, 56, doi:10.3390/en13010056.
22. Fanelli, E. CFD Hydrodynamics Investigations for Optimum Biomass Gasifier Design. *Processes* **2020**, *8*, 1323, doi:10.3390/pr8101323.
23. Karatas, H.; Akgun, F. Experimental results of gasification of walnut shell and pistachio shell in a bubbling fluidized bed gasifier under air and steam atmospheres. *Fuel* **2018**, *214*, 285–292, doi:10.1016/j.fuel.2017.10.061.
24. Meng, F.; Ma, Q.; Wang, H.; Liu, Y.; Wang, D. Effect of gasifying agents on sawdust gasification in a novel pilot scale bubbling fluidized bed system. *Fuel* **2019**, *249*, 112–118, doi:10.1016/j.fuel.2019.03.107.
25. Kumar, K.V.; Bharath, M.; Raghavan, V.; Prasad, B.; Chakravarthy, S.; Sundararajan, T. Gasification of high-ash Indian coal in bubbling fluidized bed using air and steam – An experimental study. *Appl. Therm. Eng.* **2017**, *116*, 372–381, doi:10.1016/j.applthermaleng.2017.01.102.
26. Aydar, E.; Gül, S.; Unlu, N.; Akgün, F.; Livatyali, H. Effect of the type of gasifying agent on gas composition in a bubbling fluidized bed reactor. *J. Energy Inst.* **2014**, *87*, 35–42, doi:10.1016/j.joei.2014.02.004.

27. Ren, J.; Cao, J.-P.; Zhao, X.-Y.; Yang, F.-L.; Wei, X.-Y. Recent advances in syngas production from biomass catalytic gasification: A critical review on reactors, catalysts, catalytic mechanisms and mathematical models. *Renew. Sustain. Energy Rev.* **2019**, *116*, 109426, doi:10.1016/j.rser.2019.109426.
28. Koppatz, S.; Pfeifer, C.; Hofbauer, H. Comparison of the performance behaviour of silica sand and olivine in a dual fluidised bed reactor system for steam gasification of biomass at pilot plant scale. *Chem. Eng. J.* **2011**, *175*, 468–483, doi:10.1016/j.cej.2011.09.071.
29. Zhang, K.; Yu, B.; Chang, J.; Wu, G.; Wang, T.; Wen, D. Hydrodynamics of a fluidized bed co-combustor for tobacco waste and coal. *Bioresour. Technol.* **2012**, *119*, 339–348, doi:10.1016/j.biortech.2012.05.132.
30. Yang, S.; Zhou, T.; Wei, Y.; Hu, J.; Wang, H. Influence of size-induced segregation on the biomass gasification in bubbling fluidized bed with continuous lognormal particle size distribution. *Energy Convers. Manag.* **2019**, *198*, doi:10.1016/j.enconman.2019.111848.
31. Ku, X.; Jin, H.; Lin, J. Comparison of gasification performances between raw and torrefied biomasses in an air-blown fluidized-bed gasifier. *Chem. Eng. Sci.* **2017**, *168*, 235–249, doi:10.1016/j.ces.2017.04.050.
32. Rasmussen, N.B.; Aryal, N. Syngas production using straw pellet gasification in fluidized bed allothermal reactor under different temperature conditions. *Fuel* **2020**, *263*, 116706, doi:10.1016/j.fuel.2019.116706.
33. Xue, G.; Kwapinska, M.; Horvat, A.; Kwapinski, W.; Rabou, L.; Dooley, S.; Czajka, K.; Kwapinski, W. Gasification of torrefied Miscanthus×giganteus in an air-blown bubbling fluidized bed gasifier. *Bioresour. Technol.* **2014**, *159*, 397–403, doi:10.1016/j.biortech.2014.02.094.
34. Sarker, S.; Bimbela, F.; Sanchez, J.L.; Nielsen, H.K. Characterization and pilot scale fluidized bed gasification of herbaceous biomass: A case study on alfalfa pellets. *Energy Convers. Manag.* **2015**, *91*, 451–458, doi:10.1016/j.enconman.2014.12.034.
35. Zhou, T.; Yang, S.; Wei, Y.; Hu, J.; Wang, H. Impact of wide particle size distribution on the gasification performance of biomass in a bubbling fluidized bed gasifier. *Renew. Energy* **2020**, *148*, 534–547, doi:10.1016/j.renene.2019.10.059.
36. González-Vázquez, M.P.; García, C.P.; Pevida, C.; Rubiera, F. Optimization of a Bubbling Fluidized Bed Plant for Low-Temperature Gasification of Biomass. *Energies* **2017**, *10*, 306, doi:10.3390/en10030306.
37. Prins, M.J.; Ptasinski, K.J.; Janssen, F.J. More efficient biomass gasification via torrefaction. *Energy* **2006**, *31*, 3458–3470, doi:10.1016/j.energy.2006.03.008.
38. Muvhiiwa, R.; Kuvarega, A.; Llana, E.M.; Muleja, A.A. Study of biochar from pyrolysis and gasification of wood pellets in a nitrogen plasma reactor for design of biomass processes. *J. Environ. Chem. Eng.* **2019**, *7*, 103391, doi:10.1016/j.jece.2019.103391.
39. Pio, D.; Tarelho, L.; Tavares, A.; Matos, M.; E Silva, V.B.R. Co-gasification of refused derived fuel and biomass in a pilot-scale bubbling fluidized bed reactor. *Energy Convers. Manag.* **2020**, *206*, 112476, doi:10.1016/j.enconman.2020.112476.
40. Aznar, M.P.; Caballero, M.A.; Sancho, J.A.; Francés, E. Plastic waste elimination by co-gasification with coal and biomass in fluidized bed with air in pilot plant. *Fuel Process. Technol.* **2006**, *87*, 409–420, doi:10.1016/j.fuproc.2005.09.006.
41. Cerone, N.; Zimbardi, F.; Contuzzi, L.; Baleta, J.; Cerinski, D.; Skvorčinskienė, R. Experimental investigation of syngas composition variation along updraft fixed bed gasifier. *Energy Convers. Manag.* **2020**, *221*, 113116, doi:10.1016/j.enconman.2020.113116.
42. Khezri, R.; Ghani, W.A.W.A.K.; Biak, D.R.A.; Yunus, R.; Silas, K. Experimental Evaluation of Napier Grass Gasification in an Autothermal Bubbling Fluidized Bed Reactor. *Energies* **2019**, *12*, 1517, doi:10.3390/en12081517.
43. Ge, H.; Zhang, H.; Guo, W.; Song, T.; Shen, L. System simulation and experimental verification: Biomass-based integrated gasification combined cycle (BIGCC) coupling with chemical looping gasification (CLG) for power generation. *Fuel* **2019**, *241*, 118–128, doi:10.1016/j.fuel.2018.11.091.
44. Kim, Y.D.; Yang, C.W.; Kim, B.J.; Kim, K.S.; Lee, J.W.; Moon, J.H.; Yang, W.; Yu, T.U.; Lee, U.D. Air-blown gasification of woody biomass in a bubbling fluidized bed gasifier. *Appl. Energy* **2013**, *112*, 414–420, doi:10.1016/j.apenergy.2013.03.072.
45. Arnavat, M.P.; Tora, E.; Bruno, J.C.; Coronas, A. State of the art on reactor designs for solar gasification of carbonaceous feedstock. *Sol. Energy* **2013**, *97*, 67–84, doi:10.1016/j.solener.2013.08.001.
46. Baruah, D. Modeling of biomass gasification: A review. *Renew. Sustain. Energy Rev.* **2014**, *39*, 806–815, doi:10.1016/j.rser.2014.07.129.
47. Susastriawan, A.; Saptoadi, H.; Purnomo Small-scale downdraft gasifiers for biomass gasification: A review. *Renew. Sustain. Energy Rev.* **2017**, *76*, 989–1003, doi:10.1016/j.rser.2017.03.112.
48. Marchelli, F.; Curti, M.; Tognin, M.; Rovero, G.; Moliner, C.; Arato, E.; Bosio, B. Experimental Study on the Solids Residence Time Distribution in Multiple Square-Based Spouted Beds. *Energies* **2020**, *13*, 4694, doi:10.3390/en13184694.
49. Guran, S. Thermochemical Conversion of Biomass. *Electr. Veh.* **2020**, 159–194, doi:10.1007/978-81-322-3965-9_8.
50. Hernández, J.J.; Lapuerta, M.; Barba, J.; Hernández, J.J. Separate effect of H_2, CH_4 and CO on diesel engine performance and emissions under partial diesel fuel replacement. *Fuel* **2016**, *165*, 173–184, doi:10.1016/j.fuel.2015.10.054.
51. Pérez-Navarro, Á.; Alfonso, D.S.; Ariza, H.; Cárcel-Carrasco, F.-J.; Correcher, A.; Escrivaescriva, G.; Hurtado, E.; Ibanez, F.; Peñalvo, E.; Roig, R.; et al. Experimental verification of hybrid renewable systems as feasible energy sources. *Renew. Energy* **2016**, *86*, 384–391, doi:10.1016/j.renene.2015.08.030.
52. Montuori, L.; Vargas-Salgado, C.; Alcázar-Ortega, M. Impact of the throat sizing on the operating parameters in an experimental fixed bed gasifier: Analysis, evaluation and testing. *Renew. Energy* **2015**, *83*, 615–625, doi:10.1016/j.renene.2015.04.068.
53. Alfonso-Solar, D.; Vargas-Salgado, C.; Sánchez-Díaz, C.; Hurtado-Pérez, E. Small-Scale Hybrid Photovoltaic-Biomass Systems Feasibility Analysis for Higher Education Buildings. *Sustainability* **2020**, *12*, 9300, doi:10.3390/su12219300.

54. Narváez, I.; Orío, A.; Aznar, M.P.; Corella, J. Biomass Gasification with Air in an Atmospheric Bubbling Fluidized Bed. Effect of Six Operational Variables on the Quality of the Produced Raw Gas. *Ind. Eng. Chem. Res.* **1996**, *35*, 2110–2120, doi:10.1021/ie9507540.
55. Vargas Salgado, C.A. *Estudio Comparativo de la Utilización de las Tecnologías de Gasificación Downdraft y Lecho Fluidizado Burbujeante Para la Generación de Energía Eléctrica en Aplicaciones de Baja Potencia*; Universitat Politècnica de Va-lència: Valencia, Spain, 2012.
56. Centro de estudios de la Energía. *Manuales Técnicos y de Instrucción Para la Conservación de la Energía*; Combustibles y su combustión: Madrid, Spain, 1983.
57. Bermudez, J.; Fidalgo, B. Production of bio-Syngas and bio-hydrogen via gasification. In *Handbook of Biofuels Production,* 2nd edition; Woodhead Publishing: Cambridge, UK, 2016; pp. 431–494.
58. Siedlecki, M.; De Jong, W.; Verkooijen, A.H. Fluidized Bed Gasification as a Mature And Reliable Technology for the Production of Bio-Syngas and Applied in the Production of Liquid Transportation Fuels—A Review. *Energies* **2011**, *4*, 389–434, doi:10.3390/en4030389.
59. Kunii, D.; Levenspiel, O. *Fluidization Engineering*, 2nd edition; Butterworth-Heinemann: Oxford, UK, **1991.**
60. Geldart, D. Types of Gas Fhidization. *Powder Technol*. **1973**, *7*, 285–292.
61. Kumar, A.; Jones, D.D.; Hanna, M. Thermochemical Biomass Gasification: A Review of the Current Status of the Technology. *Energies* **2009**, *2*, 556–581, doi:10.3390/en20300556.
62. Imerys Refractory Minerals. "IMERYS". Available online: https://imerys-refractoryminerals.com/europe-cis-mena/products/molochite/ (accessed on 7, October, 2019).
63. Goo, J.H.; Seo, M.W.; Kim, S.D.; Song, B.H. Effects of Temperature and Particle Size on Minimum Fluidization and Transport Velocities in a Dual Fluidized Bed. In Proceedings of the 20th International Conference on Fluidized Bed Combustion, Xi'an, China, 18–21 May 2009; Springer Science and Business Media LLC: Berlin, Germany, 2009; pp. 305–310.
64. Wen, C.Y.; Yu, Y.H. A generalized method for predicting the minimum fluidization velocity. *AIChE J.* **1966**, *12*, 610–612, doi:10.1002/aic.690120343.
65. Chirone, R.; Poletto, M.; Barletta, D.; Lettieri, P. The effect of temperature on the minimum fluidization conditions of industrial cohesive particles. *Powder Technol.* **2020**, *362*, 307–322, doi:10.1016/j.powtec.2019.11.102.
66. Lim, M.T.; Alimuddin, Z. Bubbling fluidized bed biomass gasification—Performance, process findings and energy analysis. *Renew. Energy* **2008**, *33*, 2339–2343, doi:10.1016/j.renene.2008.01.014.
67. Gómez-Barea, A.; Ollero, P.; Leckner, B. Optimization of char and tar conversion in fluidized bed biomass gasifiers. *Fuel* **2013**, *103*, 42–52, doi:10.1016/j.fuel.2011.04.042.
68. Gómez-Barea, A.; Leckner, B. Modeling of biomass gasification in fluidized bed. *Prog. Energy Combust. Sci.* **2010**, *36*, 444–509, doi:10.1016/j.pecs.2009.12.002.
69. Shi, L.; Northwood, D. The mechanical behavior of an aisi type 310 stainless steel. *Acta Met. Mater.* **1995**, *43*, 453–460, doi:10.1016/0956-7151(94)00279-q.
70. Lao, C.; Chungpaibulpatana, S. Techno-economic analysis of hybrid system for rural electrification in Cambodia. *Energy Procedia* **2017**, *138*, 524–529, doi:10.1016/j.egypro.2017.10.239.